Preparation of mesoporous SnO_2–SiO_2 composite as electrodes for lithium batteries

Fanglin Chen, Zhong Shi and Meilin Liu*

School of Materials Science and Engineering, Georgia Institute of Technology, Atlanta, GA 30332-0245, USA. E-mail: meilin.liu@mse.gatech.edu

Received (in Irvine, CA, USA) 29th March 2000, Accepted 12th September 2000
First published as an Advance Article on the web 9th October 2000

Mesoporous SnO_2–SiO_2 composite stable up to 600 °C with a BET surface area of 350 m^2 g^{-1} and an average pore size of 3.4 nm is successfully prepared, which exhibits promising cycling properties as anodes for lithium batteries.

Following the discovery of the M41S family of mesoporous silicates using supramolecular templating approach,[1,2] mesoporous materials have attracted considerable attention because of their tunable pore size, narrow pore size distribution, and remarkably large surface areas, which make them ideal candidates for catalysts, molecular sieves, and electrodes for solid-state ionic devices. The ordering in these materials is a consequence of a self-assembly process in an aqueous solution containing organic surfactants (anionic, cathodic, or neutral) and inorganic cations or anions. To date, a wide range of mesoporous materials have been prepared using the structure-directing functions of electrostatic, hydrogen-bonding, covalent bonding and van der Waals interactions associated with amphiphilic surfactant molecules.[3–10]

Tin-based composite oxides are promising candidates for anodes in lithium batteries because of their much larger reversible capacity compared to carbonaceous materials. In this study, mesoporous SiO_2 stable up to 600 °C has been prepared using Brij 56 as a structure-directing agent and TEOS as precursor in an aqueous solution.† Further, a tin compound is introduced into porous SiO_2 using a sol-gel technique to form SnO_2–SiO_2 composite. The objective of our study is to create a nano-structured SnO_2–SiO_2 electrodes for lithium batteries. The structural stability of the tin-based materials during cycling is a major barrier to the successful application of this material as anodes in Li-batteries.[11] Our approach to improving the structural stability is to incorporate a tin compound into a mesoporous SiO_2 matrix, which is structurally stable and hence offers structural stability to the nanocomposite electrode. The mesoporous SnO_2–SiO_2 structure will facilitate the penetration of the liquid electrolyte into the electrodes and hence increase the rate of charge and discharge.

Shown in Fig. 1 are XRD patterns of mesoporous SiO_2 powder samples before and after calcination at 600 °C for 2 h prepared using Brij 56 as surfactant. The XRD pattern of the as-synthesized powders indicates that the surfactant molecules were organized into a hexagonal structure when aged at room temperature for 2 d. The peak at about 1.2° corresponds to the (100) reflection, which has a *d*-spacing of 6.8 nm. Thermogravimetric analysis shows that Brij 56 surfactant is completely removed upon calcination in air at 400 °C for 1 h. The appearance of a low-angle diffraction peak of the SiO_2 powder calcined at 600 °C for 2 h indicates that mesoscopic order is preserved upon removal of the surfactant by calcination, although the structure contracted slightly as evidenced from a slight shift of the XRD peak to a higher angle. The corresponding *d*-spacing is reduced to about 6.3 nm. The increased intensity of the XRD peak of the calcined SiO_2 indicates that the ordering of the mesostructure is improved during calcination. Shown in Fig. 1(*c*) is the XRD pattern of a SnO_2–SiO_2 composite. The peak is broader than that of pure SiO_2, suggesting that either the degree of ordering was reduced or the size distribution of the mesopores was broadened. However, the position of the peak did not change, implying that the *d*-spacing remained the same upon incorporating tin species into the pores of the mesoporous SiO_2. Further, the wide-angle XRD pattern shown in the inset in Fig. 1 indicates that the SnO_2 incorporated into the mesoporous SiO_2 is crystalline, rather than amorphous.

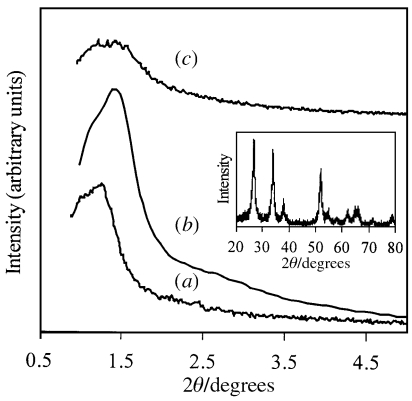

Fig. 1 Representative small-angle X-ray powder diffraction patterns of (*a*) as-synthesized SiO_2, (*b*) SiO_2 calcined at 600 °C for 2 h, and (*c*) SnO_2–SiO_2 composite calcined at 600 °C for 2 h. The wide-angle X-ray diffraction pattern of SnO_2–SiO_2 composite is shown in the inset.

Shown in Fig. 2 are representative TEM images of SiO_2 and SnO_2–SiO_2 samples after calcination at 600 °C for 2 h. Mesostructures with short-range hexagonal order can be seen and the corresponding *d*-spacings are 6.3 nm for both SiO_2 and SnO_2–SiO_2 composite, which are close to those determined from the XRD patterns. The nitrogen adsorption isotherms of the SiO_2 and SnO_2–SiO_2 samples after calcination at 600 °C for 2 h are shown in Fig. 3 and the calculated Brunauer–Emmett–Teller (BET) surface areas are 1100 m^2 g^{-1} for SiO_2 and 350 m^2 g^{-1} for SnO_2–SiO_2 composite, respectively. The gas-accessible surface area of the mesoporous SnO_2–SiO_2 composite was greatly reduced due to partial occupation of the pores by

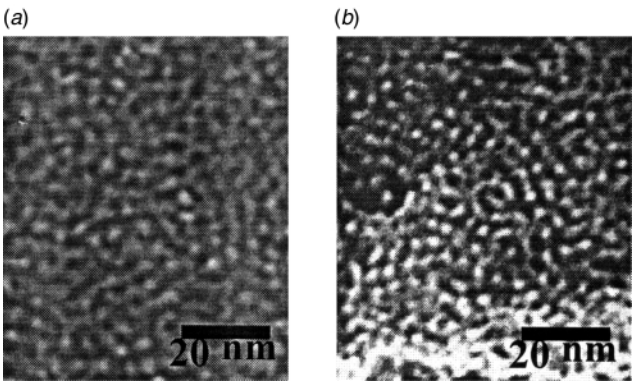

Fig. 2 TEM micrographs of (*a*) 600 °C calcined mesoporous SiO_2 and (*b*) mesoporous SnO_2–SiO_2 composite.

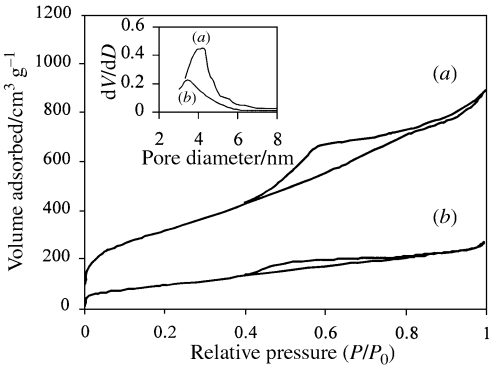

Fig. 3 Representative nitrogen adsorption and desorption isotherms for (*a*) SiO_2 and (*b*) SnO_2–SiO_2 composite after calcination at 600 °C for 2 h. Corresponding BJH pore size distributions are shown in the inset.

the tin species incorporated into the mesoporous SiO_2. Both nitogren isotherm curves have a well-defined step for the relative pressure P/P_0 ranging from 0.4 to 0.8, a characteristic of the filling of the framework-confined mesopores,[12] suggesting that both SiO_2 and SnO_2–SiO_2 samples are mesoporous after calcination at 600 °C for 2 h. As shown in the inset in Fig. 3, the average pore size in the SiO_2 structure is 4.0 nm while that in the SnO_2–SiO_2 composite is 3.4 nm, implying that a thin SnO_2 layer has been incorporated into the channel surface of the mesoporous SiO_2.

The electrochemical behavior of the obtained SnO_2–SiO_2 composite oxide is further studied using cyclic voltammetry. Shown in Fig. 4 are the cyclic voltammograms (CVs) of a mesoporous SnO_2–SiO_2 composite, as studied using a powder microelectrode in the potential range between 2.0 and 0 V (*vs.* Li^+/Li) with a scan rate of 0.2 mV s^{-1}. The potential was swept from 2.0 V in the cathodic direction down to the set limit (0 V) and then in the anodic direction. Two very small irreversible reduction peaks appeared near 0.6 and 0.9 V, respectively, in the CV of the first cycle. This is quite different from the CVs observed for tin-based composite electrodes in the literature,[13,14] in which there is only one large irreversible reduction peak around 0.9 V in the first sweep. It is well known that this large irreversible reduction peak is due to the *in situ* electrochemical reduction of SnO or SnO_2 by lithium to metallic tin and Li_2O,[15] representing a large irreversible capacity loss for tin-based composite materials in the first cycle, which is still a major barrier to the successful application of these materials as anodes in Li-batteries.[14] In this work, even though it is still not

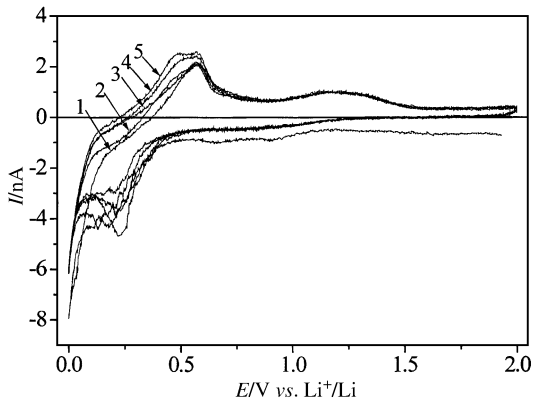

Fig. 4 Cyclic voltammograms (CVs) of a mesoporous SnO_2–SiO_2 composite as studied electrode using a powder microelectrode technique. The number adjacent to each CV represents the order of the cycles.

clear what the two tiny irreversible reduction peaks (observed for the mesoporous SnO_2–SiO_2 composite) correspond to, it is anticipated that the mesoporous SnO_2–SiO_2 composite as an anode for a lithium battery would display much less irreversible capacity loss during the first cycle. Further, the reversible redox peaks in the range of 0.1–0.7 V in the first five cycles of the CVs show very little change, an indication of good cyclability of such a mesoporous SnO_2–SiO_2 composite electrode. The electrochemical behavior of SnO_2 in mesoporous SnO_2–SiO_2 composites as well as the long-term charge–discharge cycling behavior of the composite electrodes in a lithium cell are still under investigation and will be reported in subsequent communications.

We gratefully acknowledge partial support of this research by the National Science Foundation under Award No. CTS-9819850 and by the Georgia Institute of Technology Molecular Design Institute, under prime contract N00014-95-1-1116 from the Office of Naval Research.

Notes and references

† In a typical preparation using Brij 56 as the structure-directing agent, 1.093 g Brij 56 was dissolved in 80 ml H_2O by stirring at room temperature. 2.667 g tetraethyl orthosilicate (TEOS) was added to the Brij 56 solution and the solution was stirred at room temperature for 2 h. Subsequently, 1.333 ml 0.2 M NaF was added to the above solution and the solution was stirred at room temperature for 2 h while a milky sol was obtained. The milky sol was placed at room temperature for 2 d and a white precipitate formed progressively. The precipitate was finally filtered off, washed 5 times using distilled H_2O, dried at 60 °C in a vacuum oven and finally calcined in air at 600 °C for 2 h to remove the surfactant. Incorporation of tin compound into the pores of SiO_2 was achieved by immersing mesoporous SiO_2 powder into tin nitrate solution and then drying at 40 °C under vacuum. Mesoporous SnO_2–SiO_2 composite was obtained by calcining the dried tin nitrate–SiO_2 powder at 600 °C for 2 h in air. A powder microelectrode was used to study the electrochemical performance of mesoporous SnO_2–SiO_2 composite in 1 M $LiN(SO_2CF_3)_2$/EC+DMC electrolyte solution.

1 C. T. Kresge, M. E. Leonowicz, W. J. Roth, J. C. Vartuli and J. S. Beck, *Nature*, 1992, **359**, 710.
2 J. S. Beck, J. C. Vartuli, W. J. Roth, M. E. Leonowicz, C. T. Kresge, K. D. Schmitt, C. T.-W. Chu, D. H. Olson, E. W. Sheppard, S. B. Mccullen, J. B. Higgins and J. L. Schlenker, *J. Am. Chem. Soc.*, 1992, **114**, 10 834.
3 A. Sayari, *Chem. Mater.*, 1996, **8**, 1840.
4 Z. R. Tian, W. Tong, J. Y. Wang, N. G. Duan, V. V. Krishnan and S. L. Suib, *Science*, 1997, **276**, 926.
5 Q. Huo, D. I. Margolese, U. Ciesla, D. G. Demuth, P. Feng, T. E. Gier, P. Sieger, A. Firouzi, B. F. Chmelka, F. Schuth and G. D. Stucky, *Chem. Mater.*, 1994, **6**, 1176.
6 D. M. Antonelli and J. Y. Ying, *Angew. Chem., Int. Ed. Engl.*, 1995, **34**, 2014; *Chem. Mater.*, 1996, **8**, 874; D. M. Antonelli, A. Nakahira and J. Y. Ying, *Inorg. Chem.*, 1996, **35**, 426.
7 F. Chen and M. Liu, *Chem. Commun.*, 1999, 1829.
8 D. Zhao, J. Feng, Q. Huo, N. Melosh, G. Fredrickson, B. Chmelka and G. D. Stucky, *Science*, 1998, **279**, 548.
9 E. Prouzet and T. J. Pinnavaia, *Angew. Chem., Int. Ed. Engl.*, 1997, **36**, 516.
10 P. Yang, D. Zhao, D. I. Margolese, B. F. Chemelka and G. D. Stucky, *Nature*, 1998, **396**, 152.
11 S. Machill, T. Shodai, Y. Sakuraai and J. Yamaki, *J. Power Sources*, 1998, **73**, 216.
12 S. Cabrera, J. E. Haskouri, J. Alamo, A. Beltran, D. Beltran, S. Mendioroz, M. D. Marcos and P. Amoros, *Adv. Mater.*, 1999, **11**, 379.
13 J. Li, H. Lim, Z. Wang, X. Huang and L. Chen, *J. Power Sources*, 1999, **81–82**, 346.
14 S. Machill, T. Shodai, Y. Sakurai and J. Yamaki, *J. Power Sources*, 1998, **73**, 216.
15 I. A. Courtney and J. R. Dahn, *J. Electrochem. Soc.*, 1997, **144**, 2045.